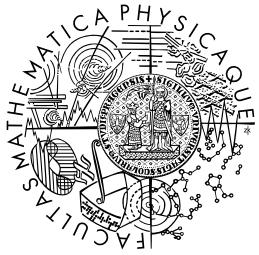


FACULTY
OF MATHEMATICS
AND PHYSICS
Charles University

**BACHELOR THESIS**

Matěj Lev Hart

# Simulating Rayleigh-Bénard convection using Smoothed Particle Hydrodynamics

Mathematical Institute of Charles University

Supervisor of the bachelor thesis: doc. RNDr. Michal Pavelka, Ph.D.
Study programme: Mathematical Modelling

Prague 2025

I declare that I carried out this bachelor thesis on my own, and only with the cited sources, literature and other professional sources. I understand that my work relates to the rights and obligations under the Act No. 121/2000 Sb., the Copyright Act, as amended, in particular the fact that the Charles University has the right to conclude a license agreement on the use of this work as a school work pursuant to Section 60 subsection 1 of the Copyright Act.

In ..... date .....  .....

Author's signature

I would like to thank my supervisor doc. Michal Pavelka for his patience and guidance throughout the work of this thesis. I would also like to thank my friends and colleagues Michael Monček and Šimon Bartoň for their support and helpful discussions.

Title: Simulating Rayleigh-Bénard convection using Smoothed Particle Hydrodynamics

Author: Matěj Lev Hart

Institute: Mathematical Institute of Charles University

Supervisor: doc. RNDr. Michal Pavelka, Ph.D., Mathematical Institute of Charles University

Abstract: We assess the suitability of Smoothed Particle Hydrodynamics (SPH) for simulating Rayleigh-Bénard convection, particularly in cryogenic helium, where the usual Boussinesq approximation fails. As a Lagrangian mesh-free method, SPH naturally accommodates large density and temperature variations, making it a strong candidate for modeling convection for non-Boussinesq fluids, such as cryogenic helium.

Keywords: Rayleigh-Bénard convection, Smoothed Particle Hydrodynamics, cryogenic helium, turbulent flow

Název práce: Simulace Rayleigh-Bénardovy konvekce pomocí Smoothed Particle Hydrodynamics

Autor: Matěj Lev Hart

Ústav: Matematický ústav UK

Vedoucí bakalářské práce: doc. RNDr. Michal Pavelka, Ph.D., Matematický ústav UK

Abstrakt: Cílem práce je prozkoumat, jestli je Smoothed Particle Hydrodynamics (SPH) vhodná metoda pro simulaci Rayleigh-Bénardovy konvekce v kryogenním heliu, kde selhává často používaná Boussinesqova approximace. SPH jako Lagrangovská bezsíťová metoda dobře pracuje s velkými rozdíly hustot a teplot v tekutině, tudíž by měla být dobrým kandidátem pro simulaci kryogenního helia.

Klíčová slova: Rayleigh-Bénárdova konvekce, Smoothed Particle Hydrodynamics, kryogenní helium, turbulentní proudění

# Contents

# Introduction

Rayleigh-Bénard convection (RBC) is a classical problem in fluid dynamics [1] [2]. It occurs when a fluid in a gravitational field is heated from below and cooled from above. This type of flow can be observed in many natural processes such as weather formation [3], oceanic flows [4], in continental drifts [5] or in convection processes in planets and stars, including the Sun [6]. The characteristic parameter describing this flow is the Rayleigh number, which determines whether or not convection occurs within the fluid. The values of Rayleigh numbers for convection in natural cases of RBC are in orders of up to $10^{30}$ [7] and even though equations describing turbulent flow are known, our ability to predict or simulate these flows, especially for such intense convection and extremely large scales, remains very limited.

Smoothed Particle Hydrodynamics (SPH) is a particle-based Lagrangian method used for the simulation of problems in fluid mechanics. The aim of this thesis is to use the SPH method to simulate RBC for high Rayleigh numbers. Particularly, using the physical parameters for cryogenic helium gas, which many experimental studies concerning RBC at high $Ra$ numbers use as their working fluid. The traditional Boussinesq approximation for RBC assumes that the physical properties of the fluid are constant except for density, where a linear relationship with temperature is taken. This approximation, however, fails for helium gas near cryogenic temperatures, since its properties vary heavily with temperature. SPH could be advantageous over other traditional grid-based methods in this regard, since omitting this approximation can be difficult for grid-based solvers, but comes naturally in the SPH method.

In the first chapter of this thesis, we derive Smoothed Particle Hydrodynamics with entropy using Poisson brackets, similarly as in Pavelka [8] and Kincl [9]. The second chapter provides a brief introduction into the physical problem of RBC. Finally, we show our numerical simulations in Julia using the SmoothedParticles.jl package developed by Kincl and Pavelka [10]. Initially for low Rayleigh numbers as a proof of concept and, if successful, for high Rayleigh numbers with the physical parameters of cryogenic helium gas.

# 1 Entropic Smoothed Particle Hydrodynamics

## 1.1 Introduction

Smoothed Particle Hydrodynamics (SPH) is a mesh-free, Lagrangian method for simulating fluid flows and continuum mechanics. Originally developed by Gingold and Monaghan (1977) [11] for astrophysical applications, SPH has since evolved into a versatile computational technique applied in fields ranging from astrophysics to engineering and computer graphics.

The core idea of SPH is to represent a continuum using a set of discrete particles, each carrying physical quantities such as mass, velocity, and energy. These quantities are interpolated over a finite support domain using smoothing kernel functions, enabling the estimation of field variables and their derivatives at any point in space [12]. Unlike traditional grid-based methods, SPH naturally handles large deformations, free-surface flows, and multiphase interactions without requiring complex mesh generation or deformation tracking.

In recent years, SPH has been increasingly applied in engineering problems, including hydrodynamics, solid mechanics, and multiphysics systems [13]. Despite its advantages, SPH faces challenges such as numerical instability, boundary treatment, and computational cost, which continue to be active areas of research.

This chapter provides a brief overview of the fundamentals of SPH including its derivation from Poisson brackets and continuum mechanics and also includes the addition of entropy to the SPH scheme for better description of non-barotropic fluids.

## 1.2 Classical Smoothed Particle Hydrodynamics

### 1.2.1 Smoothing Kernels

A fundamental component of SPH is the smoothing kernel $W_h : \mathbb{R}^d \to [0, \infty)$. The importance of the kernel is in giving weights to interactions between individual particles, as will be demonstrated later. The kernel is a function that satisfies the following properties:

- $\int W_h(\boldsymbol{x})\mathrm{d}\boldsymbol{x} = 1$
- $W_h \in C^2(\mathbb{R}^d)$
- $W_h = W_h(|\boldsymbol{x}|)$
- $h : W_h(r) = \frac{1}{h^d} W_1(\frac{r}{h})$
- $\frac{dW_h}{dr} \leq 0$

The parameter $h > 0$ is called *smoothing length*, which controls the range of interactions between particles. An important property of the kernel is that

it converges to the Dirac delta function in the sense of distributions when $h \to 0^+$. This allows approximations of functions and their spatial derivatives using convolution. Applying this property to a field variable $f$, we approximate its derivative as:

$$\begin{aligned} f &= f * \delta \approx f * W_h \\ \partial_i f &= \partial_i f * \delta \approx \partial_i f * W_h = f * \partial_i W_h \end{aligned} \tag{1.1}$$

Now we approximate the integral on the right-hand side to get a discretized expression. We can use a quadrature rule with nodes $\boldsymbol{x}_a$ and weights $V_a = \frac{m_a}{\rho_a}$ Thus we can write:

$$\begin{aligned} [f * W_h](\boldsymbol{x}_a) &= \int f(\boldsymbol{y}) W_h(\boldsymbol{x}_a - \boldsymbol{y}) d\boldsymbol{y} \approx \sum_b V_b f(\boldsymbol{x}_b) W_{h,ab} \\ [f * \partial_i W_h](\boldsymbol{x}_a) &= \int f(\boldsymbol{y}) \partial_i W_h(\boldsymbol{x} - \boldsymbol{y}) d\boldsymbol{y} \approx \sum_b V_b f(\boldsymbol{x}_b) \partial_i W_{h,ab} \end{aligned} \tag{1.2}$$

where $W_{h,ab} = W_h(\boldsymbol{x}_a - \boldsymbol{x}_b)$ is used for brevity. We will also omit the index $h$ for the same purpose. For the derivative of the kernel we get:

$$\nabla W_{ab} = \nabla W(\boldsymbol{x}_a - \boldsymbol{x}_b) = \frac{dW}{dr}(|\boldsymbol{x}_a - \boldsymbol{x}_b|) \frac{\boldsymbol{x}_a - \boldsymbol{x}_b}{|\boldsymbol{x}_a - \boldsymbol{x}_b|} \tag{1.3}$$

From the expression above, we can see that the kernel function is odd with respect to swapping of the particle indices, which will be useful later on when discussing conservational properties of SPH.

$$\nabla W_{h,ab} = -\nabla W_{h,ba} \tag{1.4}$$

The smoothing kernel should be at least twice continuously differentiable to enable the discretizations of second-order partial differential equations and operators. A natural choice for the kernel function that satisfies the properties (1.2.1) is a properly scaled Gaussian function:

$$W_h(r) = \frac{1}{(2\pi h^2)^{\frac{d}{2}}} \exp\left(-\frac{r^2}{h^2}\right), \forall r \geq 0 \tag{1.5}$$

However, Gaussian kernels have infinite support, requiring summation over all particles in the domain in 1.2, which is not computationally efficient. Thus, piece-wise polynomial functions with compact support are often used instead. A canonical example and one which we will be using in our simulations is Wendland's quintic kernel [14],

$$W_h(r) = \begin{cases} \frac{\alpha_d}{h^d}\left(1 - \frac{r}{2h}\right)^4 \left(1 + \frac{4r}{h}\right) & 0 \leq r \leq 2h \\ 0 & 2h < r \end{cases}, \tag{1.6}$$

where the normalization constant $\alpha_d$ is defined as:

$$\alpha_d = \begin{cases} \frac{3}{4} & d = 1 \\ \frac{7}{4\pi} & d = 2 \\ \frac{21}{16\pi} & d = 3 \end{cases} \tag{1.7}$$

Various other smoothing kernels exist, and interested readers can refer to [15] for more examples.

### 1.2.2 Classical approach to SPH

In the next section, we will derive the evolution equations of SPH state variables $\boldsymbol{x}_\alpha$ and $\boldsymbol{M}_\alpha$ in an elegant way using Poisson brackets and Hamiltonian continuum mechanics, closely following the formulation in Pavelka [8]. However, this is not the standard way of deriving the evolution equations in SPH literature.

The classical approach to acquiring the evolution equations can be outlined as such (Liu [16]):

1. The problem domain is approximated by a set of arbitrarily distributed particles, with no mesh or connectivity of the particles required.

2. The kernel function is used to approximate field functions via convolution.

3. The kernel approximation is further approximated using particles. The integration in the convolution is replaced by a summation over all neighboring particles in the domain of the kernel support.

4. The particle approximation is performed at every time step, which means that it is dependent on the current distribution of all the particles in the support domain.

5. All terms in the governing PDEs are rewritten using these particle-based approximations to produce a set od ODEs with respect to time.

6. The discretized set of ODEs are solved using an explicit integration scheme to track the evolution of all physical quantities per particle.

A small insight into this approach can be seen in chapter 1.2.1 concerning the smoothing kernel, particularly points 2 and 3, where the idea of using the smoothing kernel to approximate a function of state variables and its spatial derivatives was shown. The next step would be to define more rigorously how to use this approximation to discretize all terms and their spatial derivatives present in the governing equations to generate a set of ODEs with respect to time only.

However, in this thesis we will use a different approach that is described in detail in the following section.

## 1.3 Derivation of SPH based on Poisson brackets

For the derivation of the SPH equations, we will exploit the fact that SPH can be formulated within the framework of Hamiltonian continuum mechanics and, as such, can be derived via a reduction from continuum Poisson brackets. We will define SPH state variables via a mapping from their continuum counterparts, then we will plug these variables into the continuum Poisson bracket to acquire the SPH Poisson bracket. This reduced Poisson bracket will then generate the evolution equations for our state variables, once we supply the dependence of the energy functional on SPH state variables.

### 1.3.1 Lagrange and Euler frame

In the following sections, we employ the language of continuum mechanics, particularly that of the *Eulerian* and *Lagrangian* frames of reference, which offer two distinct perspectives for describing the continuum. We provide a brief overview of them below.

Suppose that we fix the origin of the frame of reference with some material point $\boldsymbol{X}$ at a specific initial time. As the material deforms, the position $\boldsymbol{X}$ does not change within this reference frame. This non-inertial frame is called the Lagrange frame (also called the material frame or reference frame). It is commonly used to describe solid materials, where the Lagrangian coordinate $\boldsymbol{X}$ tracks individual material points as they undergo deformation.

In contrast, the Eulerian frame (also called the spatial frame or current frame) is an inertial reference frame. The Eulerian coordinate $\boldsymbol{x}$ represents a fixed point in space through which we observe material flows over time. It is common to use the Eulerian frame when describing fluids, as it lends itself naturally to describing such processes. Instead of focusing on which particle is flowing through the fixed point in space at any given time, as would be the case when using the Lagrangian reference frame, the Eulerian perspective emphasizes the characteristics of the flow at that location.

Throughout this work, we adhere to the standard convention of denoting Lagrangian variables with uppercase letters (e.g., $\boldsymbol{X}$) and Eulerian variables with lowercase letters (e.g.,$\boldsymbol{x}$).

The relationship between the two reference frames and variables in the respective frames is given by the deformation mapping and its Jacobian:

$$\begin{aligned} \boldsymbol{x} &= \boldsymbol{x}(\boldsymbol{X}, t) \\ \mathrm{d}\boldsymbol{x} &= \det\frac{\partial \boldsymbol{x}}{\partial \boldsymbol{X}}\mathrm{d}\boldsymbol{X} \end{aligned} \tag{1.8}$$

### 1.3.2 Hamiltonian continuum mechanics

SPH can be formulated within the framework of Hamiltonian continuum mechanics. We use fields of position and momentum density, $x^i(\boldsymbol{X})$ and $M_i(\boldsymbol{X})$ as state variables, which are equipped with the canonical continuum Poisson bracket:

$$\{F, G\}^{Lagrangian} = \int \left( \frac{\partial F}{\partial x^i}\frac{\partial G}{\partial M_i} - \frac{\partial G}{\partial x^i}\frac{\partial F}{\partial M_i} \right) d\boldsymbol{X} \tag{1.9}$$

The evolution of any functional of these state variables is given by the Poisson bracket of the functional and the total energy $E(\boldsymbol{x}, \boldsymbol{M})$.

$$\dot{F} = \{F, E\} \tag{1.10}$$

Applying this framework to the state variables yields the canonical Hamiltonian evolution equations:

$$\dot{\boldsymbol{x}} = E_M \tag{1.11}$$

$$\dot{\boldsymbol{M}} = -E_x, \tag{1.12}$$

where $E_M, E_x$ represent partial derivatives of energy with respect to momentum or position respectively. [1]

Now we need to prescribe the total energy of the system $E(\boldsymbol{x}, \boldsymbol{M})$. We can do so using the internal energy density per Eulerian volume $\epsilon(\rho)$. The total energy is the sum of the kinetic energy and internal energy:

$$E^{Lagrangian} = \int \left( \frac{\boldsymbol{M}^2}{2\rho_0} + \det \frac{\partial \boldsymbol{x}}{\partial \boldsymbol{X}} \epsilon(\rho(\boldsymbol{x}(\boldsymbol{X}))) \right) d\boldsymbol{X}, \tag{1.13}$$

where $\rho$ is the Eulerian mass density, which is related to the Lagrangian density $\rho_0(\boldsymbol{X})$ through

$$\rho(\boldsymbol{x}) = \rho_0(\boldsymbol{X}) \det \frac{\partial \boldsymbol{X}}{\partial \boldsymbol{x}}.$$

### 1.3.3 SPH mapping

To derive the standard SPH evolution equations using Lagrangian continuum mechanics, we first need to define the SPH variables of position $\boldsymbol{x}_\alpha$ and momentum $\boldsymbol{M}_\alpha$ [2]. These discrete variables are obtained through a mapping that projects the continuous state variables onto SPH particles. The definition of this mapping follows [8].

Let $\Omega_0$ be the Lagrangian manifold, which we partition into mutually disjoint cells such that $\Omega_0 = \bigcup_\alpha \Omega_{0\alpha}$. The volume $V_{0\alpha}$ of a cell $\alpha$ is given by the integral

$$V_{0\alpha} = \int_{\Omega_{0\alpha}} d\boldsymbol{X} \tag{1.14}$$

The mapping is then given by the following equations:

$$\begin{aligned} \boldsymbol{x}_\alpha &= \int \widetilde{\chi}_\alpha(\boldsymbol{X}) \boldsymbol{x}(\boldsymbol{X}) d\boldsymbol{X} \\ \boldsymbol{M}_\alpha &= \int V_{0\alpha} \widetilde{\chi}_\alpha(\boldsymbol{X}) \boldsymbol{M}(\boldsymbol{X}) d\boldsymbol{X}, \end{aligned} \tag{1.15}$$

where

$$\widetilde{\chi}_\alpha(\boldsymbol{X}) = \begin{cases} \frac{1}{V_{0\alpha}} & \boldsymbol{X} \in \Omega_{0\alpha} \\ 0 & \text{otherwise} \end{cases} \tag{1.16}$$

is the normalized characteristic function of the Lagrangian cell $\alpha$.

To reduce the continuum Poisson bracket (1.9) to a Poisson bracket for SPH variables $\boldsymbol{x}_\alpha$ and $\boldsymbol{M}_\alpha$, we plug functionals dependent on SPH variables into the Poisson bracket. However, since the bracket contains derivatives of the functionals, we need to express the derivatives of any functional $F(\boldsymbol{x}_\alpha, \boldsymbol{M}_\alpha)$ of SPH variables with respect to the continuum state variables. From the definition of the SPH variables we can calculate the following relations:

$$\frac{\delta x^i_\alpha}{\delta x^j(\boldsymbol{X})} = \delta^i_j \widetilde{\chi}_\alpha(\boldsymbol{X}) \quad \text{and} \quad \frac{\delta M_{\alpha i}}{\delta M_j(\boldsymbol{X})} = \delta^j_i V_{0\alpha} \widetilde{\chi}_\alpha(\boldsymbol{X}) \tag{1.17}$$

[1] Actually, for elasticity, where the energy depends on the gradient of $x$, the derivatives become functional derivatives.

[2] Note the index $\alpha$, which will help us distinguish between SPH state variables and the continuous state variables

While the mixed derivatives are zero. Now we can take the derivative of a functional of SPH state variables with respect to position and momentum using the chain rule:

$$\begin{aligned}\frac{\delta F(\boldsymbol{x}_\alpha, \boldsymbol{M}_\alpha)}{\delta x^i(\boldsymbol{X})} &= \sum_\alpha \frac{\partial F}{\partial x^j_\alpha}\frac{\delta x^j_\alpha}{\delta x^i(\boldsymbol{X})} = \sum_\alpha \frac{\partial F}{\partial x^i_\alpha}\widetilde{\chi}_\alpha(\boldsymbol{X}) \\ \frac{\delta F(\boldsymbol{x}_\alpha, \boldsymbol{M}_\alpha)}{\delta M_i(\boldsymbol{X})} &= \sum_\alpha \frac{\partial F}{\partial M_{\alpha,j}}\frac{\delta M_{\alpha,j}}{\delta M_i} = \sum_\alpha \frac{\partial F}{\partial M_{\alpha,i}} V_{0\alpha}\widetilde{\chi}_\alpha(\boldsymbol{X})\end{aligned} \tag{1.18}$$

Plugging two functionals of SPH state variables into the Poisson bracket then leads to the definition of the SPH Poisson bracket:

$$\begin{aligned}\{F, G\} &= \int \left(\frac{\delta F}{\delta x^i(\boldsymbol{X})}\frac{\delta G}{\delta M_i(\boldsymbol{X})} - \frac{\delta G}{\delta x^i(\boldsymbol{X})}\frac{\delta F}{\delta M_i(\boldsymbol{X})}\right) d\boldsymbol{X} = \\ &= \sum_\alpha \sum_\beta \left(\frac{\partial F}{\partial x^i_\alpha}\frac{\partial G}{\partial M_{\beta,i}} - \frac{\partial G}{\partial x^i_\alpha}\frac{\partial F}{\partial M_{\beta,i}}\right) \int V_{0\beta}\widetilde{\chi}_\alpha(\boldsymbol{X})\widetilde{\chi}_\beta(\boldsymbol{X}) d\boldsymbol{X} \\ &= \sum_\alpha \left(F_{x^i_\alpha} G_{M_{\alpha i}} - G_{x^i_\alpha} F_{M_{\alpha i}}\right) \overset{\text{def}}{=} \{F, G\}^{\text{SPH}}\end{aligned} \tag{1.19}$$

where the following simplification using the definition of the normalized characteristic function (1.16) was used:

$$\int V_{0\beta}\widetilde{\chi}_\alpha(\boldsymbol{X})\widetilde{\chi}_\beta(\boldsymbol{X}) d\boldsymbol{X} = \int V_{0\alpha}\widetilde{\chi}^2_\alpha(\boldsymbol{X}) d\boldsymbol{X} = \int_{\Omega_{0\alpha}} \frac{1}{V^2_{0\alpha}} V_{0\alpha} d\boldsymbol{X} = \frac{1}{V_{0\alpha}} \int_{\Omega_{0\alpha}} d\boldsymbol{X} = 1$$

Furthermore, if we plug the SPH state variables into this Poisson bracket together with energy, we obtain Hamiltonian evolution equations for SPH variables, much like in classical Hamiltonian mechanics.

$$\begin{aligned}\dot{\boldsymbol{x}}_\alpha &= \{\boldsymbol{x}_\alpha, E\}^{\text{SPH}} = E_{\boldsymbol{M}_\alpha} \\ \dot{\boldsymbol{M}}_\alpha &= \{\boldsymbol{M}_\alpha, E\}^{\text{SPH}} = -E_{\boldsymbol{x}_\alpha}\end{aligned} \tag{1.20}$$

However, we still need to express the total energy in terms of $\boldsymbol{x}_\alpha, \boldsymbol{M}_\alpha$ to close the equations.

### 1.3.4 Energy functional in standard SPH formulation

To prescribe the total energy in terms of SPH variables, we need to approximate the total energy of the continuous system. Discrete particle positions and momenta are not enough to properly prescribe the energy, so we use a smoothing kernel $W$ as defined in chapter 1.2.1 to provide an approximate form of mollification. We will use smoothing kernel to define Eulerian SPH mass density, which will help us define total energy in terms of SPH variables.

$$\rho_\alpha = \sum_\beta m_\beta W(|\boldsymbol{x}_\alpha - \boldsymbol{x}_\beta|) = \sum_\beta m_\beta W_{\alpha\beta}, \tag{1.21}$$

where $m_\alpha = \int \rho_0(\boldsymbol{X})\widetilde{\chi}_\alpha(\boldsymbol{X}) d\boldsymbol{X}$ is the mass of the particle $\alpha$. Now we can close the Hamiltonian evolution equations by supplying the energy functional dependent on SPH variables:

$$E^{SPH} = \sum_\alpha V_{0\alpha} \frac{\boldsymbol{M}_\alpha^2}{2\rho_{0\alpha}} + \sum_\alpha V_{0\alpha} \frac{\rho_{0\alpha}}{\rho_\alpha} \epsilon(\rho_\alpha) \tag{1.22}$$

The equation can be simplified using the following relation: $\rho_{0\alpha} = \frac{m_\alpha}{V_{0\alpha}}$

$$E^{SPH} = \sum_\alpha \frac{\boldsymbol{M}_\alpha^2}{2m_\alpha} + \sum_\alpha V_\alpha \epsilon(\rho_\alpha)$$

When we plug this energy functional into the Hamiltonian canonical equations (1.20), we need to take its derivative with respect to the SPH variables. In particular, the derivative of $\rho_\alpha$ as defined in (1.21), which yields:

$$\begin{aligned}
\frac{\partial \rho_\beta}{\partial x_\alpha^i} &= \sum_\gamma m_\gamma W'(|\boldsymbol{x}_\beta - \boldsymbol{x}_\gamma|) \frac{\partial \sqrt{(x_\beta^j - x_\gamma^j)(x_\beta^j - x_\gamma^j)}}{\partial x_\alpha^i} \\
&= \sum_\gamma m_\gamma W'(|\boldsymbol{x}_\beta - \boldsymbol{x}_\gamma|) \frac{x_\beta^j - x_\gamma^j}{|\boldsymbol{x}_\beta - \boldsymbol{x}_\gamma|} \delta_i^j (\delta_{\beta\alpha} - \delta_{\gamma\alpha}) \\
&= \sum_\gamma m_\gamma W'_{\beta\gamma} e_{i\beta\gamma} (\delta_{\beta\alpha} - \delta_{\gamma\alpha}),
\end{aligned} \tag{1.23}$$

where $W'_{\beta\gamma} = \frac{dW}{dr}(|\boldsymbol{x}_\beta - \boldsymbol{x}_\gamma|)$ [3], and $e_{i\beta\gamma}$ is the $i$ component of the unit vector pointing from $\boldsymbol{x}_\gamma$ to $\boldsymbol{x}_\beta$, i.e. the vector $e_{\beta\gamma} = \frac{x_\beta^j - x_\gamma^j}{|\boldsymbol{x}_\beta - \boldsymbol{x}_\gamma|}$.

Now we can write the resulting ordinary differential equations for the evolution of SPH state variables given by the Poisson bracket:

$$\begin{aligned}
\dot{x}_\alpha^i &= \{x_\alpha^i, E\}^{SPH} \\
\dot{M}_{\alpha,i} &= \{M_{\alpha,i}, E\}^{SPH} \\
\dot{x}_\alpha^i &= \frac{M_\alpha^i}{m_\alpha} \\
\dot{M}_{\alpha,i} &= -\sum_\beta \left( -\frac{m_\beta}{\rho_\beta^2}\epsilon + \frac{m_\beta}{\rho_\beta}\frac{\partial \epsilon}{\partial \rho_\beta} \right) \sum_\gamma m_\gamma W'_{\beta\gamma} e_{i\beta\gamma} (\delta_{\beta\alpha} - \delta_{\gamma\alpha}) \\
&= -\sum_\beta \left( \frac{m_\alpha m_\beta}{\rho_\gamma^2} p_\alpha + \frac{m_\alpha m_\beta}{\rho_\gamma^2} p_\beta \right) W'_{\alpha\beta} e_{i\alpha\beta},
\end{aligned} \tag{1.24}$$

where the pressure of a particle $\alpha$ is defined using the barotropic relation [17]:

$$p_\alpha = -\epsilon + \rho_\gamma \frac{\partial \epsilon}{\partial \rho_\gamma} \tag{1.25}$$

When we supply the dependence of internal energy on mass density, which can be integrated from an equation of state, together with the definition of mass density 1.21 we obtain a completely specified and closed system of differential equations:

[3] This more concise notation for the derivative of the kernel will be used from here onward.

$$
\begin{aligned}
\dot{x}^i_\alpha &= \frac{M^i_\alpha}{m_\alpha} \\
\dot{M}_{\alpha i} &= -\sum_\beta \left( \frac{m_\alpha m_\beta}{\rho^2_\gamma} p_\alpha + \frac{m_\alpha m_\beta}{\rho^2_\gamma} p_\beta \right) W'_{\alpha\beta} e_{i\alpha\beta} \\
\rho_\gamma &= \sum_\beta m_\beta W_{\alpha\beta},
\end{aligned}
\tag{1.26}
$$

This system is Hamiltonian and even symplectic, since it is generated by the canonical SPH Poisson bracket 1.19 and the energy functional 1.22 [8], and thus when combined with a symplectic time integrator, such as the Verlet scheme [18], the energy error of the numerical solution is bounded uniformly with respect to time [9].

However, it should be noted that this is not the only possible way to formulate SPH. The equations (1.26) provide the evolution of equations of position and momenta and set the density as a function of the state variables. It is possible to acquire the evolution of density the same way we acquired the equations for the other state variables, i.e. using the Poisson bracket and the energy functional we obtain:

$$
\begin{aligned}
\dot{x}^i_\alpha &= \frac{M^i_\alpha}{m_\alpha} \\
\dot{M}_{\alpha i} &= -\sum_\beta \left( \frac{m_\alpha m_\beta}{\rho^2_\gamma} p_\alpha + \frac{m_\alpha m_\beta}{\rho^2_\gamma} p_\beta \right) W'_{\alpha\beta} e_{i\alpha\beta} \\
\dot{\rho}_\alpha &= \sum_\beta m_\beta W'_{\alpha\beta} \mathbf{e}_{\alpha\beta} \left( \frac{\boldsymbol{M}_\alpha}{m_\alpha} - \frac{\boldsymbol{M}_\beta}{m_\beta} \right)
\end{aligned}
\tag{1.27}
$$

This system of evolution equations is obviously different from (1.26) and they represent the standard SPH equations. While they are Hamiltonian, because they can be generated via a Poisson bracket, they are not symplectic [19]. This means that it is advantageous from a numerical perspective to evaluate the mass density at each step as a function of the other state variables, while we keep the evolution equations for positions and momenta. Doing so preserves the symplectic property of the equations and thus better energy conservation when using symplectic integrators.

However, problems arise when the fluid is not barotropic, i.e. when the density depends not only on pressure, but also on the entropy of the material. In such cases, accurately modeling the fluid dynamics requires incorporating entropy to the SPH particle description. This extension will be addressed in the following section.

## 1.4 Entropic Smoothed Particle Hydrodynamics

The classical formulation of SPH does not assign entropy to the particles. Nevertheless, for non-barotropic systems—where the internal energy depends on both density and entropy—it is advantageous to introduce entropy as an explicit variable. As a result, the energy relation in equation (1.22) takes the following modified form:

$$E^{SPH} = \sum_{\alpha} \frac{\boldsymbol{M}_{\alpha}^2}{2m_{\alpha}} + \sum_{\alpha} V_{\alpha}\epsilon(\rho_{\gamma}, s_{\alpha}), \tag{1.28}$$

where $s_\alpha$ is the Eulerian entropy density of particle $\alpha$. This entropy is itself a variable of the density of the volume. This raises a problem as particle volume in SPH can be defined in several various ways, each providing a different set of resulting evolution equations.

The definition we will be using in this thesis is the mass-based volume. We use the equation for mass density (1.21) and the definition of density itself to get:

$$(V_{\alpha})^{-1} = \frac{\rho_{\gamma}}{m_{\alpha}} \approx \sum_{\beta} \frac{m_{\beta}}{m_{\alpha}} W_{\alpha\beta} \tag{1.29}$$

This approach is standard in SPH literature as it is the simplest and usually the most stable. Other formulations exist that offer different qualities; for more detail on this matter, see Pavelka [8].

Using this definition of particle volume, we can write the definition of entropy density:

$$s_{\alpha} = S_{\alpha}(V_{\alpha})^{-1} = \frac{S_{\alpha}\rho_{\gamma}}{m_{\alpha}} \tag{1.30}$$

Finally, we can get the evolution equations of the SPH variables of $\boldsymbol{x}_\alpha$, $\boldsymbol{M}_\alpha$, $\rho_\gamma$, $s_\alpha$ by plugging these projections into the Lagrangian Poisson bracket (1.9).

$$\begin{aligned}
\dot{\boldsymbol{x}}_{\alpha} &= E_{M_{\alpha}} \\
\dot{\boldsymbol{M}}_{\alpha} &= -E_{x_{\alpha}} - \sum_{\beta} m_{\alpha} m_{\beta} \left( \frac{E_{\rho_{\alpha}}}{m_{\alpha}} + \frac{E_{\rho_{\beta}}}{m_{\beta}} + S_{\alpha} \frac{1}{m_{\alpha}^2} E_{s_{\alpha}} + S_{\beta} \frac{1}{m_{\beta}^2} E_{s_{\beta}} \right) W'_{\alpha\beta} \mathbf{e}_{\alpha\beta} \\
\dot{\rho}_{\alpha} &= \sum_{\beta} m_{\beta} W'_{\alpha\beta} \mathbf{e}_{\alpha\beta} \cdot (E_{M_{\alpha}} - E_{M_{\beta}}) \\
\dot{s}_{\alpha} &= \frac{S_{\alpha}}{m_{\alpha}} \sum_{\beta} m_{\beta} W'_{\alpha\beta} \mathbf{e}_{\alpha\beta} \cdot (E_{M_{\alpha}} - E_{M_{\beta}})
\end{aligned} \tag{1.31}$$

Now when we supply the energy functional, which is dependent on all the state variable $\boldsymbol{x}_\alpha, \boldsymbol{M}_\alpha, \rho_\gamma, s_\alpha$, (1.28) these equations result in:

$$\begin{aligned}
\dot{x}_{\alpha}^{i} &= \frac{M_{\alpha}^{i}}{m_{\alpha}} \\
\dot{M}_{\alpha i} &= -\sum_{\beta} \left( \frac{m_{\alpha} m_{\beta}}{\rho_{\alpha}^2} p_{\alpha} + \frac{m_{\alpha} m_{\beta}}{\rho_{\alpha}^2} p_{\beta} \right) W'_{\alpha\beta} e_{i\alpha\beta} \\
\dot{\rho}_{\alpha} &= \sum_{\beta} m_{\beta} W'_{\alpha\beta} \mathbf{e}_{\alpha\beta} \left( \frac{\boldsymbol{M}_{\alpha}}{m_{\alpha}} - \frac{\boldsymbol{M}_{\beta}}{m_{\beta}} \right) \\
\dot{s}_{\alpha} &= \frac{S_{\alpha}}{m_{\alpha}} \sum_{\beta} m_{\beta} W'_{\alpha\beta} \mathbf{e}_{\alpha\beta} \left( \frac{\boldsymbol{M}_{\alpha}}{m_{\alpha}} - \frac{\boldsymbol{M}_{\beta}}{m_{\beta}} \right)
\end{aligned} \tag{1.32}$$

Where pressure is defined as $p_\alpha = -\epsilon + \rho_\alpha \frac{\partial \epsilon}{\partial \rho_\alpha} + s_\alpha \frac{\partial \epsilon}{\partial s_\alpha}$ and temperature defined as $T_\alpha = \frac{\partial \epsilon}{\partial s_\alpha}$. The corresponding Poisson bracket generating these equations is defined as such:

$$
\begin{aligned}
&\{F,G\}^{\text{SPH}-\text{entropic}} = \{F,G\}^{SPH} \\
&+\sum_{\alpha}\sum_{\beta} m_\beta W'_{\alpha\beta}(F_{\rho_\gamma}(G_{M_{\alpha i}} - G_{M_{\beta i}}) - G_{\rho_\gamma}(F_{M_{\alpha i}} - F_{M_{\beta i}})) \\
&+\sum_{\alpha}\sum_{\beta} S_\alpha \frac{m_\beta}{m_\alpha} W'_{\alpha\beta} e_{i\alpha\beta}(F_{s_\alpha}(G_{M_{\alpha i}} - G_{M_{\beta i}}) - G_{s_\alpha}(F_{M_{\alpha i}} - F_{M_{\beta i}}))
\end{aligned} \tag{1.33}
$$

This Poisson bracket is obtained similarly as before. We take any two functionals of state variables $F(\boldsymbol{x}_\alpha, \boldsymbol{M}_\alpha, \rho_\gamma, s_\alpha), G(\boldsymbol{x}_\alpha, \boldsymbol{M}_\alpha, \rho_\gamma, s_\alpha)$ and we plug them into the Lagrangian Poisson bracket (1.9). In the calculation, we employ the chain rule for (functional) derivatives. We also use the result from (1.23) to evaluate the partial derivatives of density and entropy density with respect to $\boldsymbol{x}_\alpha$.

$$
\begin{aligned}
&\{F,G\} = \int \left( \frac{\delta F}{\delta x^i(\boldsymbol{X})} \frac{\delta G}{\delta M_i(\boldsymbol{X})} - \frac{\delta G}{\delta x^i(\boldsymbol{X})} \frac{\delta F}{\delta M_i(\boldsymbol{X})} \right) d\boldsymbol{X} = \\
&= \sum_{\alpha,\beta,\gamma,\xi} \int \left( \left[ \frac{\partial F}{\partial x^j_\alpha} \frac{\partial x^j_\alpha}{\partial x^i(\boldsymbol{X})} + \frac{\partial F}{\partial M_{\beta,j}} \frac{\partial M_{\beta,j}}{\partial x^i(\boldsymbol{X})} + \frac{\partial F}{\partial \rho_\gamma} \frac{\partial \rho_\gamma}{\partial x^i(\boldsymbol{X})} + \frac{\partial F}{\partial s_\xi} \frac{\partial s_\xi}{\partial x^i(\boldsymbol{X})} \right] \right. \\
&\cdot \left[ \frac{\partial G}{\partial M_{\beta,j}} \frac{\partial M_{\beta,j}}{\partial M_i(\boldsymbol{X})} + \frac{\partial G}{\partial x^j_\alpha} \frac{\partial x^j_\alpha}{\partial M_i(\boldsymbol{X})} + \frac{\partial G}{\partial \rho_\gamma} \frac{\partial \rho_\gamma}{\partial M_i(\boldsymbol{X})} + \frac{\partial G}{\partial s_\xi} \frac{\partial s_\xi}{\partial M_i(\boldsymbol{X})} \right] \\
&- \left[ \frac{\partial G}{\partial x^j_\alpha} \frac{\partial x^j_\alpha}{\partial x^i(\boldsymbol{X})} + \frac{\partial G}{\partial M_{\beta,j}} \frac{\partial M_{\beta,j}}{\partial x^i(\boldsymbol{X})} + \frac{\partial G}{\partial \rho_\gamma} \frac{\partial \rho_\gamma}{\partial x^i(\boldsymbol{X})} + \frac{\partial G}{\partial s_\xi} \frac{\partial s_\xi}{\partial x^i(\boldsymbol{X})} \right] \\
&\left. \cdot \left[ \frac{\partial F}{\partial M_{\beta,j}} \frac{\partial M_{\beta,j}}{\partial M_i(\boldsymbol{X})} + \frac{\partial F}{\partial x^j_\alpha} \frac{\partial x^j_\alpha}{\partial M_i(\boldsymbol{X})} + \frac{\partial F}{\partial \rho_\gamma} \frac{\partial \rho_\gamma}{\partial M_i(\boldsymbol{X})} + \frac{\partial F}{\partial s_\xi} \frac{\partial s_\xi}{\partial M_i(\boldsymbol{X})} \right] \right) d\boldsymbol{X}
\end{aligned}
$$

We now use the relations (1.17), (1.23) and the definition of entropy through density to simplify the expression:

$$
\begin{aligned}
&= \sum_{\alpha,\beta,\gamma,\xi} \int \left( \left[ \frac{\partial F}{\partial x^i_\alpha} \widetilde{\chi}_\alpha(\boldsymbol{X}) + \frac{\partial F}{\partial \rho_\gamma} \sum_\phi m_\phi W'_{\gamma\phi} e_{i\gamma\phi}(\delta_{\gamma\beta} - \delta_{\phi\beta}) \widetilde{\chi}_\beta(\boldsymbol{X}) + \right. \right. \\
&\left. + \frac{\partial F}{\partial s_\xi} \frac{S_\xi}{m_\xi} \sum_\theta m_\theta W'_{\xi\theta} e_{i\xi\theta}(\delta_{\xi\beta} - \delta_{\theta\beta}) \widetilde{\chi}_\beta(\boldsymbol{X}) \right] \cdot \left[ \frac{\partial G}{\partial M_{\beta,i}} V_{0\beta} \widetilde{\chi}_\beta(\boldsymbol{X}) \right] \\
&- \left[ \frac{\partial G}{\partial x^i_\alpha} \widetilde{\chi}_\alpha(\boldsymbol{X}) + \frac{\partial G}{\partial \rho_\gamma} \sum_\phi m_\phi W'_{\gamma\phi} e_{i\gamma\phi}(\delta_{\gamma\beta} - \delta_{\phi\beta}) \widetilde{\chi}_\beta(\boldsymbol{X}) + \right. \\
&\left. \left. + \frac{\partial G}{\partial s_\xi} \frac{S_\xi}{m_\xi} \sum_\theta m_\theta W'_{\xi\theta} e_{i\xi\theta}(\delta_{\xi\beta} - \delta_{\theta\beta}) \widetilde{\chi}_\beta(\boldsymbol{X}) \right] \cdot \left[ \frac{\partial F}{\partial M_{\beta,i}} V_{0\beta} \widetilde{\chi}_\beta(\boldsymbol{X}) \right] \right) d\boldsymbol{X}
\end{aligned}
$$

Where the partial derivatives of density and entropy density with respect to momentum vanish. Now if we reorganize the terms and use the previous result (1.3.3) to take out the integral with the characteristic functions, the whole expression becomes clearer:

$$
\begin{aligned}
&= \sum_\beta \left[ \left( \sum_\alpha F_{x_\alpha^i} G_{M_{\beta,i}} - F_{M_\beta,i} G_{x_\alpha^i} \right) + \right. \\
&+ \left( \sum_\gamma F_{\rho_\gamma} G_{M_{\beta,i}} - F_{M_{\beta,i}} G_{\rho_\gamma} \sum_\phi m_\phi W'_{\gamma\phi} e_{i\gamma\phi} (\delta_{\gamma\beta} - \delta_{\phi\beta}) \right) + \\
&+ \left. \left( \sum_\xi F_{s_\xi} G_{M_{\beta,i}} - F_{M_{\beta,i}} G_{s_\xi} \frac{S_\xi}{m_\xi} \sum_\theta m_\theta W'_{\xi\theta} e_{i\xi\theta} (\delta_{\xi\beta} - \delta_{\theta\beta}) \right) \right] \\
&= \{F, G\}^{SPH} + \\
&+ \sum_\beta \sum_\gamma \sum_\phi m_\phi W'_{\gamma\phi} e_{i\gamma\phi} (\delta_{\gamma\beta} - \delta_{\phi\beta}) (F_{\rho_\gamma} G_{M_{\beta,i}} - F_{M_{\beta,i}} G_{\rho_\gamma}) + \\
&+ \sum_\beta \sum_\xi \sum_\theta \frac{S_\xi}{m_\xi} m_\theta W'_{\xi\theta} e_{i\xi\theta} (\delta_{\xi\beta} - \delta_{\theta\beta}) (F_{s_\xi} G_{M_{\beta,i}} - F_{M_{\beta,i}} G_{s_\xi}) \\
&= \{F, G\}^{SPH} + \\
&+ \sum_\gamma \sum_\phi m_\phi W'_{\gamma\phi} e_{i\gamma\phi} (F_{\rho_\gamma} (G_{M_{\gamma,i}} - G_{M_{\phi,i}}) - G_{\rho_\gamma} (F_{M_{\gamma,i}} - F_{M_{\phi,i}})) \\
&+ \sum_\xi \sum_\theta \frac{S_\xi}{m_\xi} m_\theta W'_{\xi\theta} e_{i\xi\theta} (F_{s_\xi} (G_{M_{\xi,i}} - G_{M_{\theta,i}}) - G_{s_\xi} (F_{M_{\xi,i}} - F_{M_{\theta,i}}))
\end{aligned}
$$

Which after relabeling $(\gamma, \phi)$ and $(\xi, \theta)$ to $(\alpha, \beta)$ is precisely the Poisson bracket (1.33).

The equations (1.32) represent the complete evolution equations of the reversible, Hamiltonian parts of state variables $\boldsymbol{x}_\alpha, \boldsymbol{M}_\alpha, \rho_\gamma, s_\alpha$. When we use the update relation for the density $\rho_\gamma = \sum_\beta m_\beta W_{\alpha\beta}$, which directly corresponds to the evolution equation for density in (1.32) [4], this system is even symplectic [8]. Thus, when we use a symplectic integrator for this system, we conserve a certain energy $E^*$, which is close to the real energy. Since these equations represent the reversible part of the evolution, total entropy $s_\alpha$ should be conserved. It is indeed so:

$$
\dot{s} = \sum_\alpha \dot{s}_\alpha = \sum_\alpha \frac{S_\alpha}{V_\alpha} \sum_\beta m_\beta W'_{\alpha\beta} \mathbf{e}_{\alpha\beta} \cdot (E_{M_\alpha} - E_{M_\beta}) = 0 \tag{1.34}
$$

The total sum is equal to zero due to the anti-symmetry of the kernel derivative with respect to indices (1.3).

## 1.5 Entropic SPH with dissipative evolution

We also include irreversible dissipative processes in our simulation, namely Fourier heat conduction and viscous dissipation, and the following section will briefly introduce the mechanics by which we incorporate these into our SPH scheme.

One possible way of adding Fourier heat conduction is based on a dissipation potential. This approach stems from the General Equation for Non-Equilibrium

[4] This follows from taking the time derivative of the definition relation for the density and using the equation for $\dot{x}_\alpha^i$.

Reversible-Irreversible Coupling (GENERIC) [17] [20] [21]. The details of the calculation are beyond the scope of this work, thus we only include the resulting evolution part of entropy and refer the reader to [8, 17] for a rigorous derivation of this equation.

$$(\dot{S}_\alpha)_{\text{Fourier}} = V_\alpha \frac{\partial s_\alpha}{\partial \epsilon_\alpha} \dot{\epsilon}_\alpha = -\epsilon_\alpha^* \sum_\beta V_\alpha V_\beta (\boldsymbol{q}_\alpha + \boldsymbol{q}_\beta) \cdot W'_{\alpha\beta} \mathbf{e}_{\alpha\beta} \tag{1.35}$$

Here, $\epsilon_\alpha^* = T_\alpha^{-1}$ is the SPH inverse temperature of particle $\alpha$, and the discrete heat flux $\boldsymbol{q}_\alpha$ is given by

$$\boldsymbol{q}_\alpha = -\sum_\beta V_\beta \lambda_F \left( T_\alpha - \frac{T_\alpha^2}{T_\beta} \right) W'_{\alpha\beta} \mathbf{e}_{\alpha\beta} \tag{1.36}$$

with $\lambda(T_\alpha) = \lambda_F T_\alpha^2$ following the discretization scheme outlined in [8]. This formulation ensures compliance with the second law of thermodynamics, as the entropy production is guaranteed to be non-negative by construction of the dissipation potential.

Similarly, we also include viscous dissipation following the standard SPH discretization of the viscous terms:

$$(\dot{S}_\alpha)_{\text{viscous}} = -\frac{1}{T_\alpha} \sum_\beta (n+2) \mu V_\alpha V_\beta ((\boldsymbol{v}_\alpha - \boldsymbol{v}_\beta) \cdot \mathbf{e}_{\alpha\beta})^2 \frac{W'_{\alpha\beta}}{r_{\alpha\beta}} \tag{1.37}$$

as derived in [8] [11]. This expression corresponds to the irreversible transfer of kinetic energy into internal energy via viscous friction, where $\mu$ is the dynamic viscosity, and the geometric factor $(n+2)$ arises from the specific discretization of the dissipation potential in particle-based form.

In both cases, the entropy production rates $\dot{S}_\alpha$ are directly added to the evolution of the Lagrangian particle entropies $S_\alpha$, ensuring consistent thermodynamic behavior while preserving energy conservation in the GENERIC framework.

# 2 Rayleigh-Bénard convection

Rayleigh-Bénard convection [1] is a classical problem in fluid dynamics [2] [1]. It is a buoyancy-driven flow that occurs when a fluid in a gravitational field is heated from below and cooled from above. This phenomenon can be seen naturally in many different areas and scales. Some examples include weather formation, flows within the Earth's crust, oceanic flows and many more. The physical problem we will be investigating in this thesis can be defined as follows [22].

## 2.1 Problem definition

Let us have a closed container with walls being non-deformable free surfaces with vertical height $L$ and horizontal diameter $D$, defining an aspect ratio $\Gamma = \frac{D}{L}$. Inside the box, we have a viscous heat conducting fluid subject to gravitational acceleration $g$ in the downward direction. The fluid is heated from below with temperature $T_h$ and cooled from above with temperature $T_c$.

When the temperature difference between the two surfaces $\Delta T = T_h - T_c$ is below a critical value, no flows occur and heat is spread only by conduction. However, after crossing some critical value $\Delta T^*$ this conductive state becomes unstable and flows begin to form. In rectangular containers, these flows take the form of regular rolls parallel to the short side of the container. Note that the direction of flow in these rolls is unpredictable and two adjacent rolls rotate in the opposite directions [22].

Why do flows begin to form? When the fluid is heated from below, temperature gradients form within the fluid layers, which in turn produce a density gradient. A fluid droplet that is close to the hot lower plate has a lower density than the rest of the layer, as density generally decreases with temperature. As long as there are no disturbances within the fluid layer, it is surrounded by particles with the same density and the forces acting upon the droplet are balanced and thus it remains stationary. Now let us assume that, due to some local fluctuation, the droplet is displaced upward. Since it is now less dense than its surroundings, buoyant forces push it upward, reinforcing its motion. This positive feedback leads to the onset of convective flow.

This interpretation would suggest that convection ensues whenever there exists a temperature gradient in the fluid. However, we know from experience that this is not the case. The reason for this is that there exist stabilizing forces that oppose this buoyant motion. One of them is the viscosity of the fluid, which generates a friction force directly opposite to the motion. The other is heat diffusion, which spreads out the heat contained within the droplet to its surrounding environment, reducing the temperature and thus density difference. This gives us an idea of why there exists a critical temperature $\Delta T^*$ for which convection occurs. For lower temperatures, the buoyant forces are not strong enough to overcome the dissipative effects and vice versa for higher temperatures.

However, temperature alone does not determine whether fluid flows will occur. As previously noted, there exist opposing internal forces within the fluid, includ-

[1] referred to as 'RBC' from here on out

ing heat dissipation and viscous resistance, which act to suppress the onset of convection. Consequently, the initiation of convection does not depend solely on a critical temperature difference, but also on the physical properties of the fluid, such as its kinematic viscosity $\nu$, and thermal diffusivity $\kappa$. To account for these combined effects, the Rayleigh number $Ra$ is introduced as the dimensionless parameter that governs the onset of convection. It is defined as:

$$Ra = g\frac{\alpha}{\nu\kappa}\Delta T L^3, \tag{2.1}$$

Here $g$ is the gravitational acceleration and $\Delta T$ is the difference in temperature between the top and bottom plates separated by the vertical distance $L$. In geophysical and astrophysical contexts, where the problem dimensions and temperature differences are large, Rayleigh numbers can reach values as high as $10^{30}$ [7].

In addition to the Rayleigh number, the Prandtl number $Pr$ plays an important role when discussing flows in RBC. It is defined as the ratio of the kinematic viscosity $\nu$ and the thermal diffusivity $\kappa$.

$$Pr = \frac{\nu}{\kappa} \tag{2.2}$$

Low-Prandtl-number fluids (e.g. liquid metals, where $Pr \ll 1$) have fast heat diffusion compared to momentum diffusion, which leads to different flow structures compared to high-Prandtl-number fluids. For fluids where $Pr \approx 1$ (e.g. many gases including helium), the thermal and momentum diffusivities are comparable, which simplifies scaling analysis and makes these fluids ideal for researching these relations.

Apart from the onset of convection, a central focus of RBC research is the efficiency of heat transport, which is quantified by the dimensionless Nusselt number $Nu$, which compares total heat transfer to purely conductive heat transfer. It is defined as:

$$Nu = \frac{LH}{\lambda\Delta T}, \tag{2.3}$$

where $H$ is the total convective heat flux and $\lambda$ the thermal conductivity of the fluid. This convective heat transfer and its dependency on the Rayleigh number, especially for very high values of $Ra$ is an integral property of RBC and has been a subject of numerous studies. For moderate Rayleigh numbers (up to about $10^{11}$), experiments across a wide range of working fluids have shown consistent scaling behavior; however, for higher values of $Ra$, strong differences appear and call for further experimental and numerial research [7].

To achieve very high Rayleigh numbers in controlled laboratory settings, many researchers use cryogenic helium gas as their working fluid, since its physical properties, namely its kinematic viscosity $\nu$, thermal expansion coefficient $\alpha$ and thermal diffusivity $\kappa$ allow for very high Rayleigh numbers (up to $10^{15}$) even in laboratory settings [23].

## 2.2 Physical regimes and scaling laws

As the Rayleigh number increases beyond the critical value $Ra_c$, the behavior of the system transitions through distinct regimes. When $Ra$ values are just above $Ra_c$, the flow is steady and organized in the form of laminar convection rolls. As $Ra$ increases further, the flows become more chaotic and the system enters the turbulent regime where thermal plumes dominate heat transport. The scaling laws governing the Nusselt number in this regime are of particular interest, expressed as:

$$Nu \propto Ra^{\gamma} Pr^{\beta}, \tag{2.4}$$

In the classical turbulent regime, where $\gamma = 1/3$ [24], boundary layers remain laminar even as the bulk of the fluid becomes turbulent. In contrast, the so-called "ultimate regime" proposed by Kraichnan [25] predicts a steeper scaling $\gamma = 1/2$. The idea behind the ultimate regime is that at sufficiently high $Ra$ values, the laminar boundary layers near the heating walls break down and become turbulent themselves, meaning that convective heat transfer dominates, leading to a steeper scaling. These transitions remain an active area of research, including experiments for RBC with high Rayleigh numbers with cryogenic helium [23].

## 2.3 Boussinesq approximation

A common approximation that is used when modeling RBC is the Boussinesq approximation. We assume that for small temperature differences, fluid properties vary little with temperature. The approximation then lies in assuming that fluid properties other than density are constant, and a linear relationship with temperature is assumed for the density:

$$\rho(T) = \rho_0[1 - \alpha(T - T_0)], \tag{2.5}$$

where $\alpha$ is the coefficient of thermal expansion. When this approximation is applied to the Navier-Stokes equations, we get the following system:

$$\begin{aligned} \nabla \cdot \mathbf{t} - \rho_0 \alpha (T - T_0)\vec{g} &= \rho_0 \frac{D\vec{v}}{Dt} \\ \mathbf{t} &= -p\mathbf{I} + \nu(\nabla\vec{v} + (\nabla\vec{v})^T) \\ \nabla \cdot \vec{v} &= 0 \\ \frac{\partial T}{\partial t} &= -\vec{v} \cdot \nabla T + \kappa \nabla \cdot (\nabla T), \end{aligned} \tag{2.6}$$

where $\mathbf{t}$ is the Cauchy stress tensor and $\nu$ is the kinematic viscosity. The reason why we are introducing this topic is to highlight why SPH may be advantageous when simulating RBC. In the SPH method, density is evolved dynamically through the evolution equations (1.32), so there is no need for a linear approximation. This is important for our goal of simulating cryogenic helium gas since, at very low temperatures (around 5 K), helium exhibits strongly non-Boussinesq behavior due to its highly varying thermophysical properties in that area. This highlights why SPH may be advantageous for simulating helium, since direct numerical

simulations of confined RBC without the Boussinesq approximation for very high Rayleigh numbers are difficult [26].

# 3 Numerical Simulations

Our numerical simulations are performed using SmoothedParticles package for Julia developed by Ondřej Kincl [27][28][29]. Our goal was to try to simulate RBC with cryogenic helium gas as our working fluid. We use the HEPAK program written in Fortran [30], which allows us to get various physical parameters of cryogenic helium needed for our simulation.

## 3.1 Simulation parameters

We use a convection cell with an aspect ratio $\Gamma = \frac{D}{L} = 4$. The reference pressure $p_0$ is set to 100000 Pa. The temperature of the top plate is set to 5 K, with the temperature difference $\Delta T = 0.05K$. We set the physical properties of the fluid to that of cryogenic helium gas at the aforementioned temperature and pressure values using data from HEPAK 3.1.

| | Unit | Values |
|---|---|---|
| Heat capacity $C_V$ | $J/K$ | 3159 |
| Reference density $\rho_0$ | $Kg/m^3$ | 11.78 |
| Thermal expansion coefficient $\alpha$ | $m/K$ | 1.631 |
| Thermal diffusivity $\kappa$ | $m^2/s$ | $1.29 \cdot 10^{-7}$ |
| Speed of sound $c_0$ | $m/s$ | 117.7 |
| Dynamic viscosity $\mu$ | $Pa \cdot s$ | $1.39 \cdot 10^{-6}$ |
| Heat conductivity $\lambda$ | $W/(m \cdot K)$ | 0.01022 |

**Table 3.1** Physical properties of helium at the working conditions

## 3.2 Equation of state

Our first attempts at the simulation used the stiffened gas model [31], which gives the following thermodynamic relation for the volumetric energy density:

$$\epsilon = \rho \left( \frac{c_0^2}{\gamma(\gamma-1)} \left( \frac{\rho}{\rho_0} \right)^{\gamma-1} e^{\frac{s}{c_V \rho}} + \frac{\rho_0 c_0^2 - \gamma p_0}{\gamma \rho} \right), \tag{3.1}$$

where $\rho_0, p_0$ and $c_0$ are the reference density, pressure, and speed of sound, $\gamma = \frac{c_P}{c_v}$ is the ratio of heat capacity at constant pressure to heat capacity at constant volume, and $s$ is the volumetric entropy density. The following equations then follow from this relation:

$$p = (\gamma - 1)\epsilon - (\rho_0 c_0^2 - \gamma p_0) \tag{3.2}$$

$$T = \frac{c_0^2}{c_V \gamma(\gamma-1)} \left( \frac{\rho}{\rho_0} \right)^{\gamma-1} e^{\frac{s}{c_V \rho}} \tag{3.3}$$

$$\mu = \frac{c_0^2}{\gamma - 1} \left( \frac{\rho}{\rho_0} \right)^{\gamma-1} e^{\frac{s}{c_V \rho}} - \rho \frac{c_0^2}{\gamma(\gamma-1)} \left( \frac{\rho}{\rho_0} \right)^{\gamma-1} \frac{s}{\rho^2 c_V} \tag{3.4}$$

In particular, if we set $\rho = \rho_0$, $p = p_0$, we get $s = 0$ and then the equation of state becomes:

$$p = (\gamma - 1)\rho c_V T - \frac{\rho_0 c_0^2 - \gamma p_0}{\gamma} \tag{3.5}$$

However, under closer investigation, we have found that the pressure and density values acquired using this equation of state do not fit the data from HEPAK, nor have any other standard equation of state we found. For this reason, we decided to do a quadratic fit of energy density as a function of entropy and density to use as an equation of state and to derive expressions for pressure and temperature using standard thermodynamic relations. The justification of why a quadratic fit should be sufficient is that we are working within a small area of pressure and temperature values and thus a simpler model fitted to that area should suffice.

We acquired 100 values of density as well as energy and entropy per unit mass from HEPAK for temperature and pressure values in ranges relevant to our experiment ($T \approx 5$ K, $P \approx 100000$ Pa). We then fitted the energy density as a quadratic function of entropy density and density using the least squares method.

$$e(\rho, s) = e_0 + \alpha s + \beta\rho + \gamma s\rho + \delta\rho^2 + \varepsilon s^2 \tag{3.6}$$

The resulting coefficients are:

| | |
|---|---|
| $e_0$ | $8.4539 \cdot 10^4$ |
| $\alpha$ | $-1.4338 \cdot 10^1$ |
| $\beta$ | $-2.6828 \cdot 10^3$ |
| $\gamma$ | $3.7663 \cdot 10^{-1}$ |
| $\delta$ | $-1.2070 \cdot 10^1$ |
| $\varepsilon$ | $7.7031 \cdot 10^{-4}$ |

**Table 3.2** Fitted coefficients

We then use standard thermodynamic relations to get the expressions for pressure and temperature, as well as other parameters needed for the simulation [22].

$$\begin{aligned} T &= \left(\frac{\partial e}{\partial s}\right) = \alpha + \gamma\rho + 2\varepsilon s \\ P &= \rho^2 \left(\frac{\partial e}{\partial \rho}\right)_= \rho^2(\beta + \gamma s + 2\delta\rho) \\ c &= \sqrt{\left(\frac{\partial p}{\partial \rho}\right)} = 2\rho(\beta + \gamma s + 2\delta\rho) + 2\delta\rho^2 \\ C_v &= \frac{1}{T^2}\left(\frac{\partial^2 s}{\partial e^2}\right)^{-1} = \frac{((\gamma\rho + \alpha)^2 - 4\varepsilon(e_0 + \beta\rho + \delta\rho^2 - e))^{\frac{3}{2}}}{2\varepsilon(\alpha + \gamma\rho + 2\varepsilon s)^2} \end{aligned} \tag{3.7}$$

The equations for energy and temperature hold reasonably well, with the mean % error being less than 1 % for energy per unit mass and temperature and around 2 % for pressure and 3 % for the speed of sound. Heat capacity error was considerably larger at around 14 %, most likely because of the second derivative

not being as accurate for our quadratic fit. For comparison, the stiffened gas model was in some cases off by more than $\approx 20$ %. In the future, we can use higher-order fits or more data for a more accurate model.

| | Maximum error [%] | Mean error [%] |
|---|---|---|
| Energy | 0.125 | 0.045 |
| Temperature | 4.025 | 0.982 |
| Pressure | 6.101 | 2.249 |
| Speed of sound | 4.372 | 3.219 |
| Heat capacity | 26.077 | 14.538 |

**Table 3.3** % Error of the fitted quadratic model

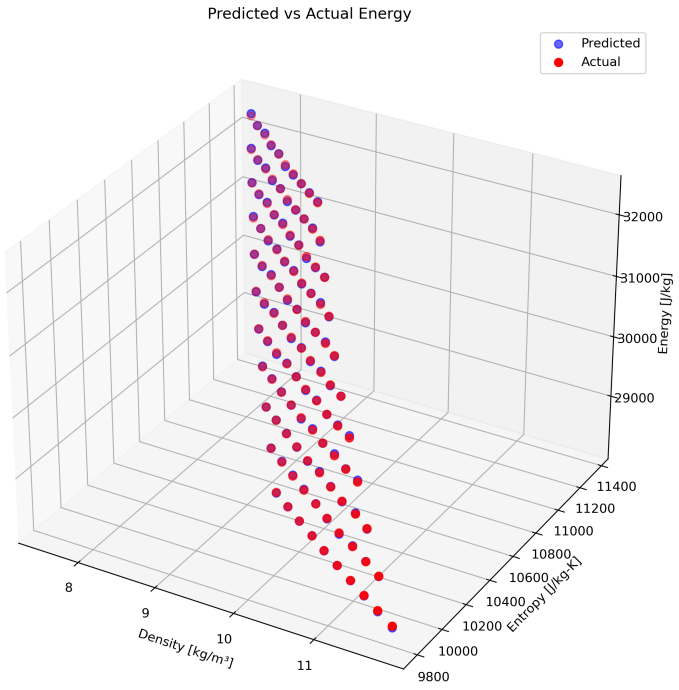


**Figure 3.1** Energy surface from the fitted model together with original data points.

## 3.3 Test Simulations

Before simulating helium as our working fluid, we ran test simulations to verify the functionality of the model. We used the stiffened gas equation of state as well as the derived thermodynamic relations. As outlined above, we used a convection cell with aspect ratio $\Gamma = 4$, with heating from below and a constant temperature at the top layer. We ran a number of simulations with temperature differences ranging from $\Delta T = 20$K to 400K. We were able to produce the characteristic 'plume' shapes [32] present in turbulent RBC, as can be seen in the figure 3.2. After a stabilization period, we can see that the flows take the form of parallel rolls as can be seen in the figures 3.3 3.4. Consistent with theory, for low Rayleigh numbers no flows occurred within the fluid and heat propagated through the fluid

only by conduction 3.5 3.6. It should be noted that the results from the test simulations are illustrative and should be taken as qualitative at best, since some non-physical parameters were used.

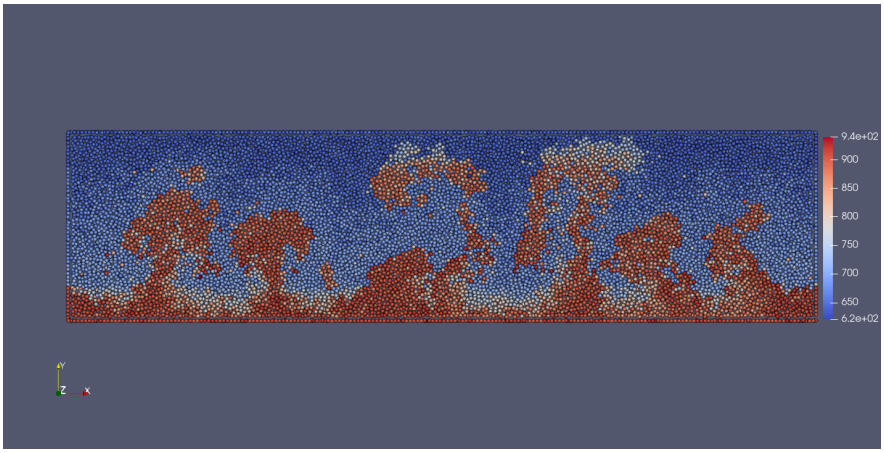


**Figure 3.2** Plume shapes of flows in RBC at t = 1s, Ra = $2.1 \cdot 10^{10}$

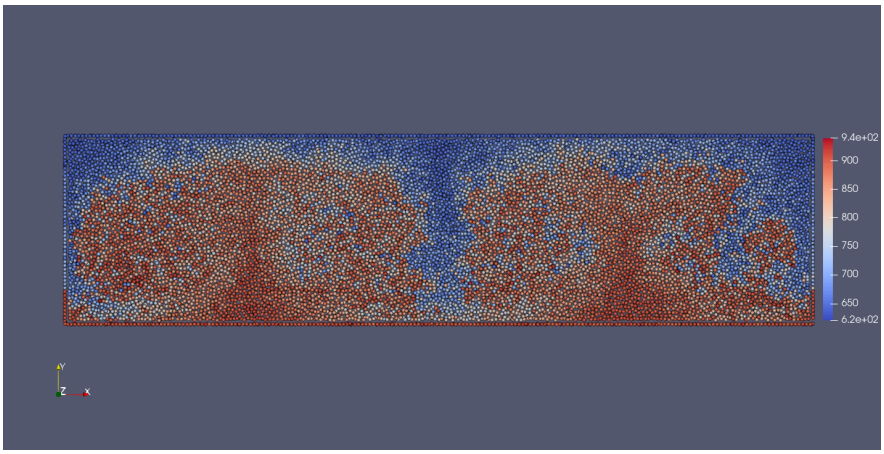


**Figure 3.3** Lateral convection rolls in RBC at t = 9s, Ra = $2.1 \cdot 10^{10}$

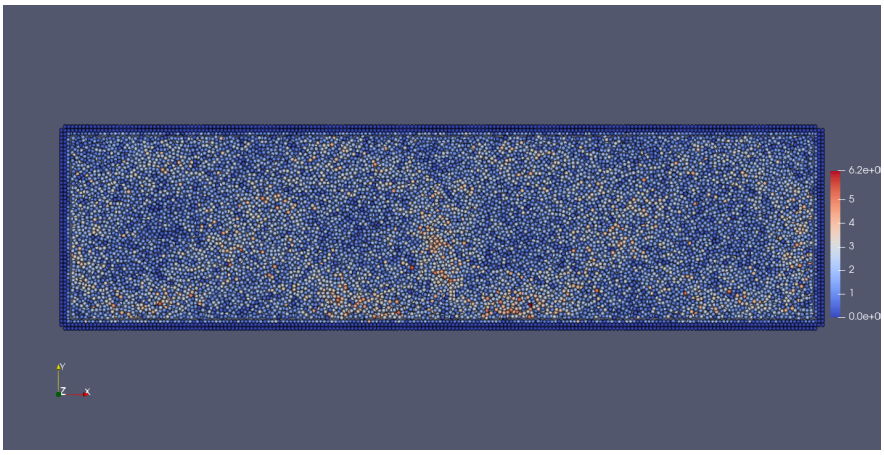


**Figure 3.4** Velocity magnitude of RBC at t = 9s. Notice the visible rings, where convection rolls occur, Ra = $2.1 \cdot 10^{10}$

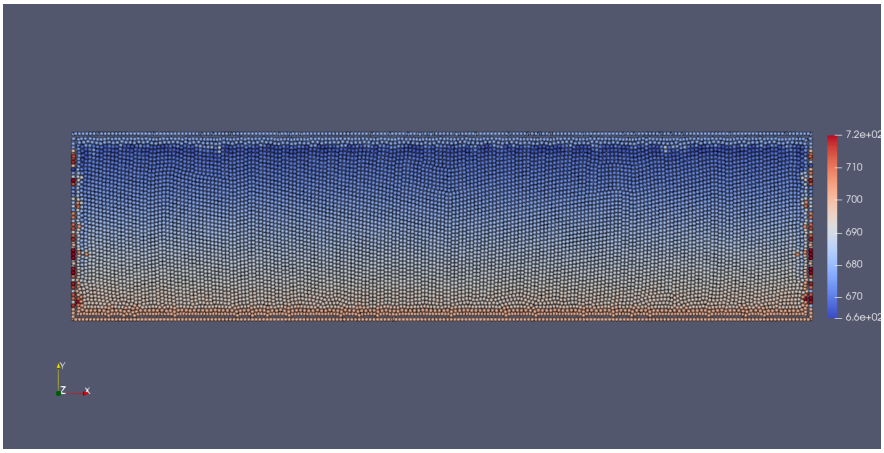


**Figure 3.5** Temperature gradient as a result of conduction in simulation with low Rayleigh number. Some particles on the boundary have a higher temperature due to the LJ energy boundary implementation. This however had no significant impact on the bulk of the simulation.

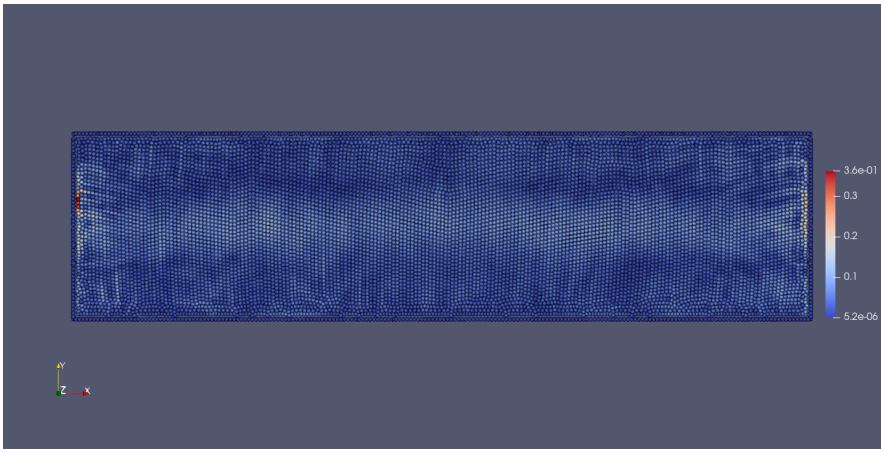


**Figure 3.6** Velocity magnitude in simulation with low Rayleigh number. t = 10s

## 3.4 Helium simulation problems

During our simulations, particularly when trying to simulate cryogenic helium, we have encountered a number of difficulties, some inherent to the SPH method, others with our implementation.

### 3.4.1 Tensile instability

Tensile instability is a common numerical artifact in SPH. It is primarily caused by negative pressure states. When the particles are subjected to tensile stress, the interpolation kernel causes particles to clump together in chains and overall causes unphysical behavior and numerical instability. There are a number of ways to deal with tensile instability. A common one is adding an artificial background pressure term to prevent states with negative pressure [33] or adding a repulsive term to particles that are too close [34]. There are also other more sophisticated ways that attempt to deal with tensile instability, including an adaptive kernel [35] or even adding an artificial term to energy, exploiting the conservational properties

of SPH [29].

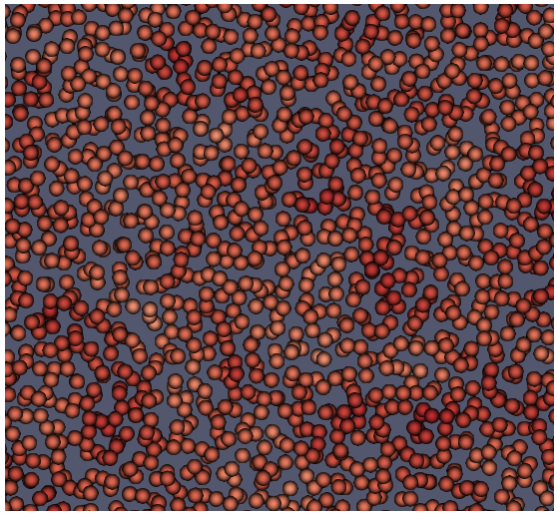

**Figure 3.7** Example of tensile instability in the simulation

### 3.4.2 Boundary problems

In simulations of cryogenic helium, the extremely low dynamic viscosity of the fluid ($\mu \approx 1 \cdot 10^{-6}$ Pa$\cdot$s) resulted in very high velocities and kinetic energies of the particles. This led to particles escaping the wall boundaries since they possessed sufficient momentum to overcome the confining potential. In the simulations, the boundary wall conditions were implemented using a repulsive Lennard-Jones (LJ) potential to model particle-wall interactions. By increasing the wall energy parameter as well as the wall thickness, the strength and spatial extent of the LJ force was sufficient to stop particles from escaping.

## 3.5 Summary

In summary, we have been able to use SPH to simulate the qualitative features of RBC, namely the difference in regimes for simulations with different Ra values, where for large Ra values we observed typical plume-shaped flows within the fluid and after a stabilization period we observed the lateral rolls; and for low values of Ra, no flows occurred and heat was transferred throughout the fluid by conduction only. We encountered difficulties when trying to adapt the simulation to parameters of cryogenic helium due to tensile instability and small dynamic viscosity, resulting in very large velocities and particles escaping.

The stiffened gas equation of state proved to be inadequate for cryogenic helium at the range of temperatures and pressures we were trying to simulate. To compensate for this, we found a quadratic fit of energy per unit mass as a function of density and entropy per unit mass fitted to data acquired from HEPAK [30]. This fit proved to be reasonably consistent with other values derived from the equation of state via standard thermodynamical relations.

The adaptation of the simulation to that of cryogenic helium proved to be more difficult than expected and we were unable to produce relevant results due

to the instability of the simulation. We believe, that a combination of some of the ways of tackling tensile instability presented earlier could resolve this issue and allow for better simulations.

# Conclusion

This thesis serves as an overview of the SPH method in the context of simulating Rayleigh-Bénard convection, and we hope that it can serve as a starting point for future investigation in simulating cryogenic helium.

In the first chapter, we recalled the SPH method, and we derived the governing equations by exploiting the fact that SPH can be formulated within the framework of Hamiltonian continuum mechanics and reducing the continuum Poisson bracket, closely following the formulation in [8]. We derived a full set of symplectic equations for the reversible part of the evolution, including entropy, which allows for the use of symplectic integrators, such as the Verlet scheme [18]. We also include irreversible dissipative terms such as Fourier heat conduction and viscous dissipation.

The second chapter presented the physical framework of Rayleigh-Bénard convection [2] [1]. We defined the physical problem which we investigated and provided an insight into what causes flows to begin forming within the fluid. We also introduced the physical parameters that govern the regimes of flows within the fluid and briefly discussed the problem of scaling laws between the Nusselt number and Rayleigh number in turbulent regimes for very high Rayleigh numbers. We also commented on the Boussinesq approximation and why SPH is well suited for simulating the problem without this approximation, since it naturally avoids it.

In the final chapter, we discussed the results of our numerical simulations. We first described the parameters of our simulation setup, including the physical data taken from [30]. The initial attempts at modeling the fluid used the stiffened gas equation of state; however, we found that this model poorly approximated the thermodynamic behaviour of helium at cryogenic conditions, with significant deviations in data such as temperature and pressure when compared to HEPAK data. To address this issue, we used a fitted equation of state acquired from a quadratic least-squares fit of internal energy as a function of density and entropy using data from HEPAK, which proved to be consistent in the relevant temperature and pressure regions.

We then presented the results of our test simulations using the stiffened gas model, which qualitatively captured the features of Rayleigh-Bénard convection, including plume formations and convection rolls at high Rayleigh numbers and no flows forming for low Rayleigh numbers. However, when trying to adapt the simulation to cryogenic helium, we encountered numerical instabilities, particularly tensile instability, which is unfortunately a common numerical artifact in SPH. These results provide insight into the strengths and weaknesses of the SPH method and help us understand what necessary steps are needed to make future simulations more stable.

Despite these challenges, the results demonstrate the capability of SPH to capture the essential dynamics of RBC and highlight the main obstacles in simulating cryogenic helium. Future work may benefit implementing more robust stabilization techniques to improve numerical stability. We hope this work may provide a solid basis for such developments.

# Bibliography


1. Rayleigh, Lord. LIX. On convection currents in a horizontal layer of fluid, when the higher temperature is on the under side. *The London, Edinburgh, and Dublin Philosophical Magazine and Journal of Science*. 1916, vol. 32, no. 192, pp. 529–546.
2. Bénard, Henri. Les tourbillons cellulaires dans une nappe liquide. *Revue Gen. Sci. Pure Appl.* 1900, vol. 11, pp. 1261–1271.
3. Hartmann, Dennis L.; Moy, Leslie A.; Fu, Qiang. Tropical convection and the energy balance at the top of the atmosphere. *Journal of Climate*. 2001.
4. Marshall, John; Schott, Friedrich. Open-ocean convection: Observations, theory, and models. *Reviews of Geophysics*. 1999.
5. Mackenzie, D.P.; Roberts, J.M.; Weiss, N. Convection in the Earth's mantle: towards a numerical simulation. *Journal of Fluid Mechanics*. 1974.
6. Cattaneo, F.; Emonet, T.; Weiss, N. On the interaction between convection and magnetic fields. *The Astrophysical Journal*. 2003.
7. Urban, Pavel; Hanzelka, Pavel; Musilová, Věra; Králík, Tomáš; Mantia, Marco La; Srnka, Aleš; Skrbek, Ladislav. Heat transfer in cryogenic helium gas by turbulent Rayleigh–Bénard convection in a cylindrical cell of aspect ratio 1. *New Journal of Physics*. 2014.
8. Pavelka, Michal; Klika, Václav; Kincl, Ondřej. *Approaches to conservative Smoothed Particle Hydrodynamics with entropy*. 2024. Available from arXiv: `2406.14229 [physics.flu-dyn]`.
9. Kincl, Ondřej. *Extension of smoothed particle hydrodynamics based on Poisson brackets*. 2024. PhD thesis. Charles University.
10. Kincl, Ondřej; Pavelka, Michal. *github.com/OndrejKincl/SmoothedParticles.jl* [N.d.]. Parallelized library for smoothed particle hydrodynamics (SPH) in 2d and 3d.
11. Gingold, R. A.; Monaghan, J. J. Smoothed particle hydrodynamics: theory and application to non-spherical stars. *Monthly Notices of the Royal Astronomical Society*. 1977.
12. Monaghan, Joe J. Smoothed particle hydrodynamics. *In: Annual review of astronomy and astrophysics. Vol. 30 (A93-25826 09-90), p. 543-574*. 1992, vol. 30, pp. 543–574.
13. Liu, MB; Liu, GR2593940. Smoothed particle hydrodynamics (SPH): an overview and recent developments. *Archives of computational methods in engineering*. 2010, vol. 17, pp. 25–76.
14. Wendland, Holger. Piecewise polynomial, positive definite and compactly supported radial functions of minimal degree. *Advances in computational Mathematics*. 1995.
15. Violeau, Damien. *Fluid Mechanics and the SPH Method: Theory and Applications*. Oxford University Press, 2012.

16. Liu, G.R.; Liu, M.B. *Smoothed Particle Hydrodynamics: A Meshfree Particle Method*. 2003. ISBN 9789812384560. Available from DOI: 10.1142/5340.

17. Pavelka, Michal; Klika, Václav; Grmela, Miroslav. *Multiscale Thermo-Dynamics: Introduction to GENERIC*. De Gruyter, 2018. ISBN 9783110350951. Available from DOI: 10.1515/9783110350951.

18. Hairer, Ernst; Lubich, Christian; Wanner, Gerhard. Geometric numerical integration illustrated by the Störmer–Verlet method. *Acta numerica*. 2003, vol. 12, pp. 399–450.

19. Jerrold E. Marsden, Tudor S. Ratiu. *Introduction to Mechanics and Symmetry*. Springer New York, NY, 1999.

20. Grmela, Miroslav; Öttinger, Hans Christian. Dynamics and thermodynamics of complex fluids. I. Development of a general formalism. *Physical Review E*. 1997, vol. 56, no. 6, p. 6620.

21. Öttinger, Hans Christian; Grmela, Miroslav. Dynamics and thermodynamics of complex fluids. II. Illustrations of a general formalism. *Physical Review E*. 1997, vol. 56, no. 6, p. 6633.

22. G. Lebon D. Jou, J. Casas-Vázquez. *Understanding Non-equilibrium Thermodynamics*. Springer Berlin, Heidelberg, 2008.

23. Urban, Pavel; Králík, Tomáš; Musilová, Věra; Skrbek, Ladislav. Modulated turbulent convection: a benchmark model for large scale natural flows driven by diurnal heating. *Scientific Reports*. 2024, vol. 14, no. 1, p. 15987.

24. Malkus, Willem VR. The heat transport and spectrum of thermal turbulence. *Proceedings of the Royal Society of London. Series A. Mathematical and Physical Sciences*. 1954, vol. 225, no. 1161, pp. 196–212.

25. Kraichnan, Robert H. Turbulent Thermal Convection at Arbitrary Prandtl Number. *Phys. Fluids 5 1374–89*. 1962.

26. Ahlers, Guenter; Grossmann, Siegfried; Lohse, Detlef. Heat transfer and large scale dynamics in turbulent Rayleigh-Bénard convection. *Rev. Mod. Phys.* 2009.

27. Kincl, Ondřej; Pavelka, Michal. Globally time-reversible fluid simulations with smoothed particle hydrodynamics. *Computer Physics Communications*. 2023, vol. 284, p. 108593.

28. Kincl, Ondřej; Schmoranzer, David; Pavelka, Michal. Simulation of superfluid fountain effect using smoothed particle hydrodynamics. *Physics of Fluids*. 2023, vol. 35, no. 4.

29. Kincl, Ondřej; Peshkov, Ilya; Pavelka, Michal; Klika, Václav. Unified description of fluids and solids in Smoothed Particle Hydrodynamics. *Applied Mathematics and Computation*. 2023, vol. 439, p. 127579.

30. Hands, BA; Arp, V; McCarty, RD. HEPROP-88: A computer code for helium properties. In: *Proceedings of the Twelfth International Cryogenic Engineering Conference Southampton, UK, 12–15 July 1988*. Elsevier, 1988, pp. 460–463.

31. Dumbser, Michael; Peshkov, Ilya; Romenski, Evgeniy; Zanotti, Olindo. High order ADER schemes for a unified first order hyperbolic formulation of continuum mechanics: viscous heat-conducting fluids and elastic solids. *Journal of Computational Physics*. 2016, vol. 314, pp. 824–862.

32. Ahlers, Guenter; Grossmann, Siegfried; Lohse, Detlef. Heat transfer and large scale dynamics in turbulent Rayleigh-Bénard convection. *Reviews of modern physics*. 2009, vol. 81, no. 2, pp. 503–537.

33. Bui, Ha H; Fukagawa, Ryoichi; Sako, Kazunari; Ohno, Shintaro. Lagrangian meshfree particles method (SPH) for large deformation and failure flows of geomaterial using elastic–plastic soil constitutive model. *International journal for numerical and analytical methods in geomechanics*. 2008, vol. 32, no. 12, pp. 1537–1570.

34. Monaghan, Joseph J. SPH without a tensile instability. *Journal of computational physics*. 2000, vol. 159, no. 2, pp. 290–311.

35. Lahiri, Saptarshi Kumar; Bhattacharya, Kanishka; Shaw, Amit; Ramachandra, LS. A stable SPH with adaptive B-spline kernel. *Journal of Computational Physics*. 2020, vol. 422, p. 109761.